Available online at www.sciencedirect.com
ScienceDirect
Journal of Power Sources 165 (2007) 678–684
JOURNAL OF POWER SOURCES
www.elsevier.com/locate/jpowsour

Ni–Fe + SDC composite as anode material for intermediate temperature solid oxide fuel cell

X.C. Lu, J.H. Zhu *

Department of Mechanical Engineering, Box 5014, Tennessee Technological University, TN 38505, USA

Received 1 July 2006; received in revised form 13 December 2006; accepted 14 December 2006
Available online 3 January 2007

Abstract

Composite materials of $Sm_{0.2}Ce_{0.8}O_{1.9}$ (SDC) with various Ni–Fe alloys were synthesized and evaluated as the anode for intermediate temperature solid oxide fuel cell. The performance of single cells consisting of the Ni–Fe + SDC anode, SDC buffer layer, $La_{0.8}Sr_{0.2}Ga_{0.83}Mg_{0.17}O_{2.815}$ (LSGM) electrolyte, and $SrCo_{0.8}Fe_{0.2}O_{3-\delta}$ (SCF) cathode were measured in the temperature range of 600–800 °C with wet H_2 as fuel. It was found that the anodic overpotentials of the different Fe–Ni compositions at 800 °C were in the following order: $Ni_{0.8}Fe_{0.2} < Ni_{0.75}Fe_{0.25} < Ni < Ni_{0.7}Fe_{0.3} < Ni_{0.9}Fe_{0.1} < Ni_{0.95}Fe_{0.05} < Ni_{0.33}Fe_{0.67}$. The single cell with the $Ni_{0.8}Fe_{0.2}$ + SDC anode exhibited a maximum power density of 1.43 W cm^{-2} at 800 °C and 0.62 W cm^{-2} at 700 °C. The polarization resistance of the $Ni_{0.8}Fe_{0.2}$ + SDC anode was as low as 0.105 Ω cm^2 at 800 °C under open circuit condition. A stable performance with essentially negligible increase in anode overpotential was observed during about 160 h operation of the cell with the $Ni_{0.8}Fe_{0.2}$ + SDC anode at 800 °C with a fixed current density of 1875 mA cm^{-2}. The possible mechanism responsible for the improved electrochemical properties of the composite anodes with the $Ni_{0.8}Fe_{0.2}$ and $Ni_{075}Fe_{0.25}$ alloys was discussed.

Keywords: Solid oxide fuel cell; Alloy; Anode; Polarization resistance

1. Introduction

Solid oxide fuel cell (SOFC), which uses solid oxides as electrolyte, is a device that can convert chemical energy directly into electricity. SOFC possesses some unique advantages over the traditional power generation technologies, including inherently high efficiency, low greenhouse emissions and fuel flexibility. A number of chemicals such as H_2, natural gas (CH_4 with small mounts of other hydrocarbons), alcohols, dimethyl ether (DME), and other hydrocarbons have been used as fuels in SOFC [1–5].

Ni has been widely used as anode material since it has good electrical conductivity and high catalytic ability towards H_2 oxidation. However, due to its thermal expansion mismatch with electrolyte and particle coarsening at high temperatures, Ni is usually mixed with an oxide conductor such as yttria-stabilized zirconia (YSZ) to form a composite anode [6]. Another advantage of this composite anode is that the triple-phase boundary (TPB) can be dramatically extended from the anode/electrolyte interface into the anode. As a result, the electrochemical activity of Ni towards H_2 oxidation reaction is enhanced and the anode polarization resistance is reduced [7,8].

One of the major problems of SOFC is the excessively high working temperature which might cause problems such as anode particle coarsening during long-term operation, crack formation due to thermal expansion mismatch between cell components, and rapid degradation in cell performance due to interdiffusion between various cell materials. However, with decreasing operation temperature the cell power density decreases significantly, especially below 700 °C. The losses of power density come from the high internal resistance of electrolyte and polarization resistance of electrodes. Recently, the perovskite phase (La, Sr) (Ga, Mg)O_3 has been proposed as an alternative electrolyte material [9–14]. It was reported that the electrical conductivity of $La_{0.8}Sr_{0.2}Ga_{0.83}Mg_{0.17}O_{2.815}$ (LSGM) was about 0.17 S cm^{-1} at 800 °C, i.e. four times higher than that of YSZ. Also, LSGM was shown to have negligible electronic conductivity at temperatures below 1000 °C over a broad range of O_2 partial pressures from 10^{-21} to 0.1 MPa [15,16]. Therefore, LSGM is a promising electrolyte material for intermediate temperature SOFC.

* Corresponding author. Tel.: +1 931 372 3186; fax: +1 931 372 6340.
E-mail address: jzhu@tntech.edu (J.H. Zhu).

0378-7753/$ – see front matter © 2007 Elsevier B.V. All rights reserved.
doi:10.1016/j.jpowsour.2006.12.047

As for high performance anodes, doped ceria, particularly samaria-doped ceria ($Sm_{0.2}Ce_{0.8}O_{1.9}$, SDC) together with Ni is most commonly used due to the high ionic conductivity of SDC at intermediate temperature [1,9,17–20]. The electrochemical and catalytic properties of Ni might be improved by partially replacing Ni with other metals such as Fe, Co and Cu [21,22]. Ringuedé et al. reported [21] that by adding Co to the Ni–YSZ composite anode the cell performance was improved. Small fractions of Cu also had a positive effect on the anodic electrochemical activities. Shinagawa et al. [22] studied several Ni–Fe bimetallic anodes operating on H_2 fuel. Enhancement in anodic property of Ni by a small amount of Fe addition was found. With an addition of 5 wt.% Fe to Ni, the anodic overpotential was reduced to almost half of that for pure Ni. In the Ni–Fe alloy system, an intermetallic phase Ni_3Fe existed below 517 °C in the composition range of 10–36 wt.% Fe [23]. Wan et al. [24] found that the H_2 molecules were easily adsorbed and desorbed on the surface of an ordered Ni_3Fe phase at room temperature. Ni_3Fe was also chemically active towards the decomposition of hydrogen molecules. Even though the ordered phase Ni_3Fe is unstable in the temperature range of 600–800 °C of interest to SOFC, local short-range ordering might still exist in this composition range and as a result these alloys might exhibit unique anodic behaviors.

In this work, the electrochemical properties of a series of $Ni_{1-x}Fe_x$ + SDC ($x = 0$, 0.05, 0.1, 0.2, 0.25, 0.3 and 0.67) composite anodes were evaluated at intermediate temperature using a LSGM electrolyte supported cell configuration. Some Ni–Fe alloy compositions were identified which exhibited low polarization resistance and are therefore potential anode materials.

2. Experimental

2.1. Synthesis of cell components

A series of mixed Ni–Fe oxide powders were prepared using the glycine-nitrate process. First, stoichiometric amounts of $Ni(NO_3)_2$ (99.95%, Sigma–Aldrich) and $Fe(NO_3)_3$ (98+%, Sigma–Aldrich) were dissolved in distilled water. The amounts of $Ni(NO_3)_2$ and $Fe(NO_3)_3$ were controlled such that the Fe content in the Ni–Fe alloy will be 0, 5, 10, 20, 25, 30, 67 wt.% after reduction. After glycine (NH_2–CH_2–COOH, 99.5+%, Alfa Aesar) was added to the solution, it was boiled to evaporate excess water. The resulting viscous liquid was ignited and underwent combustion, producing an ash composed of oxide products. The ash was then fired at 900 °C for 2 h to remove possible carbon residues. The SDC powders were prepared in a similar way, starting with $Ce(NO_3)_3$ (99.5%, Alfa Aesar) and $Sm(NO_3)_3$ (99.9%, Aldrich). Finally, the Ni–Fe oxide powders and the SDC powders (the weight percentage of the reduced metal was about 50 wt.%) were thoroughly mixed and ball-milled as the anode material.

LSGM with a composition of $La_{0.8}Sr_{0.2}Ga_{0.83}Mg_{0.17}O_{2.815}$ was selected as the electrolyte, which was prepared by solid-state reaction. La_2O_3 (99.99%, Alfa Aesar), $SrCO_3$ (99.99%, Alfa Aesar), Ga_2O_3 (99.999%, Alfa Aesar) and MgO (99.99%, Alfa Aesar) were used as starting materials. Precalcination of starting materials, La_2O_3 and MgO, at 1000 °C for 10 h was conducted in order to remove the hydroxides and carbonates among them, while $SrCO_3$ and Ga_2O_3 were dried at 120 °C for 1 h. Stoichiometric amounts of pre-treated La_2O_3, $SrCO_3$, Ga_2O_3 and MgO were mixed evenly in an agate mortar with the aid of acetone. After mixing, the powders were pelletized, fired at 1250 °C for 5 h and ground with mortar and pestle. This process was repeated twice, followed by ball-milling to reduce the powder size. Finally, the powders were pelletized and sintered at 1470 °C for 10 h. The pellets were then ground and polished to a thickness of 300 μm for single cell tests.

$SrCo_{0.8}Fe_{0.2}O_{3-\delta}$ (SCF) was selected as the cathode because of its excellent mixed ionic/electronic conductivity and good coupling with the LSGM electrolyte. It was also prepared by conventional solid-state reaction. Stoichiometric amounts of $SrCO_3$, CoO and Fe_2O_3 were mixed, pelletized and then sintered at 1100 °C for three times. The SCF powders were finally balled-milled to reduce the particle size.

2.2. Cell fabrication

The (Ni–Fe + SDC)/SDC/LSGM/SCF single cells were prepared as follows. A thin layer of SDC was deposited on one side of the LSGM electrolyte by screen printing a slurry of the SDC ink and drying at 150 °C on a hot plate. The composite anode was screen printed atop the SDC interlayer. The double layers together with Pt-mesh current collector were annealed at 1300 °C for 0.5 h. The thickness of the interlayer and the anode layer was 10 and 15–20 μm, respectively. The SCF cathode layer was screen printed on the opposite side of LSGM electrolyte with a similar procedure and was fired at 1100 °C for 0.5 h. The thickness of the cathode was 20 μm. The effective working electrode area was 0.24 cm^2. Reference electrodes consisting of the same materials as working electrodes were deposited on the LSGM disc about 2.5 mm away from working electrodes. The reference electrodes were used to monitor the overpotentials of the anode and cathode.

2.3. Cell characterization

The composite anode powders were first fired at 1300 °C and then reduced in H_2 with 3% H_2O at 800 °C, followed by quenching to room temperature by removing the powders away from the hot zone. The phases in the reduced powders were identified by powder X-ray diffraction (XRD). The cross-sectional microstructures of various anodes after cell testing were examined by scanning electron microscopy (SEM, FEI XL30 environmental scanning electron microscope). The single cell tests were carried out using an electrochemical interface (Solartron 1287, Solartron Analytical) with a LabView program in the temperature range of 600–800 °C. The electrochemical impedance spectra (EIS) of the single cells were measured with the electrochemical interface and a frequency response analyzer (Solartron 1260, Solartron Analytical) under open circuit condition (OCV). The frequency range was from 2 MHz to 0.005 Hz and the ac amplitude was 10 mV. A double-layer glass sealing design was used in all our single cell tests as previously described

[25]. The assembled cells were placed in the hot zone of a vertical furnace. Wet fuel (H_2 with 3% H_2O) was fed to the anode surface at a rate of 30 ml min^{-1} and stationary air was used as oxidant at the cathode side.

3. Results and discussion

3.1. Phase identification and microstructure of the Ni–Fe + SDC anodes

XRD results show that two phases (a FCC Ni–Fe solid solution and a cubic SDC phase) were present in all the Ni–Fe + SDC anode powders after reduction in H_2 with 3% H_2O followed by rapid cooling, as shown in Fig. 1(a)–(e). This result is consistent with the Ni–Fe phase diagram, which indicates that Ni and Fe are completely soluble at elevated temperatures [23]. The peaks from the solid solution shifted slightly to the lower angles with the increasing addition of Fe to Ni.

Typical cross-sectional views of the fractured cells near the anode side after cell operation are shown in Fig. 2. The SDC interlayer was quite dense and uniform with a thickness of about 10 μm. The Ni–Fe + SDC layers of about 15–20 μm thick were relatively porous after reduction. Strong bonding between all the anodes and the electrolytes was achieved. No obvious differences in microstructure were noticed among these Ni–Fe + SDC anodes.

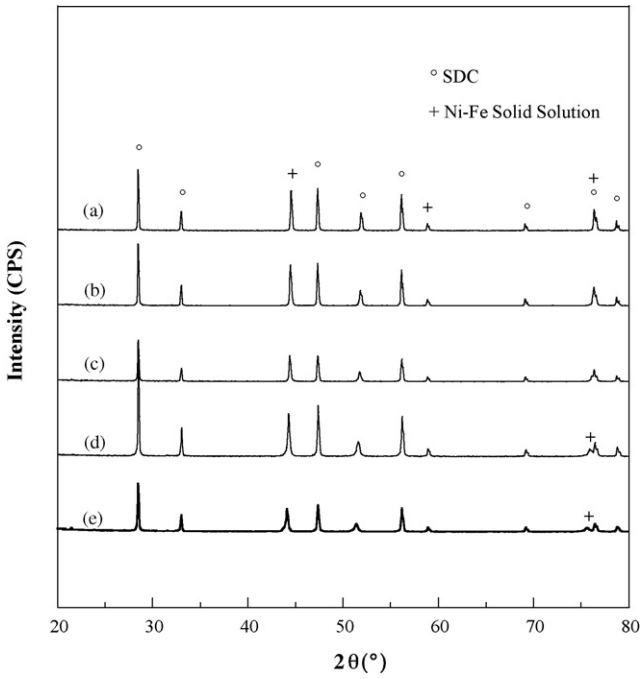

Fig. 1. XRD patterns of some Ni–Fe + SDC composites after reduction in H_2 + 3% H_2O followed by quenching to room temperature: (a) Ni + SDC; (b) $Ni_{0.95}Fe_{0.05}$ + SDC; (c) $Ni_{0.9}Fe_{0.1}$ + SDC; (d) $Ni_{0.8}Fe_{0.2}$ + SDC; (e) $Ni_{0.75}Fe_{0.25}$ + SDC.

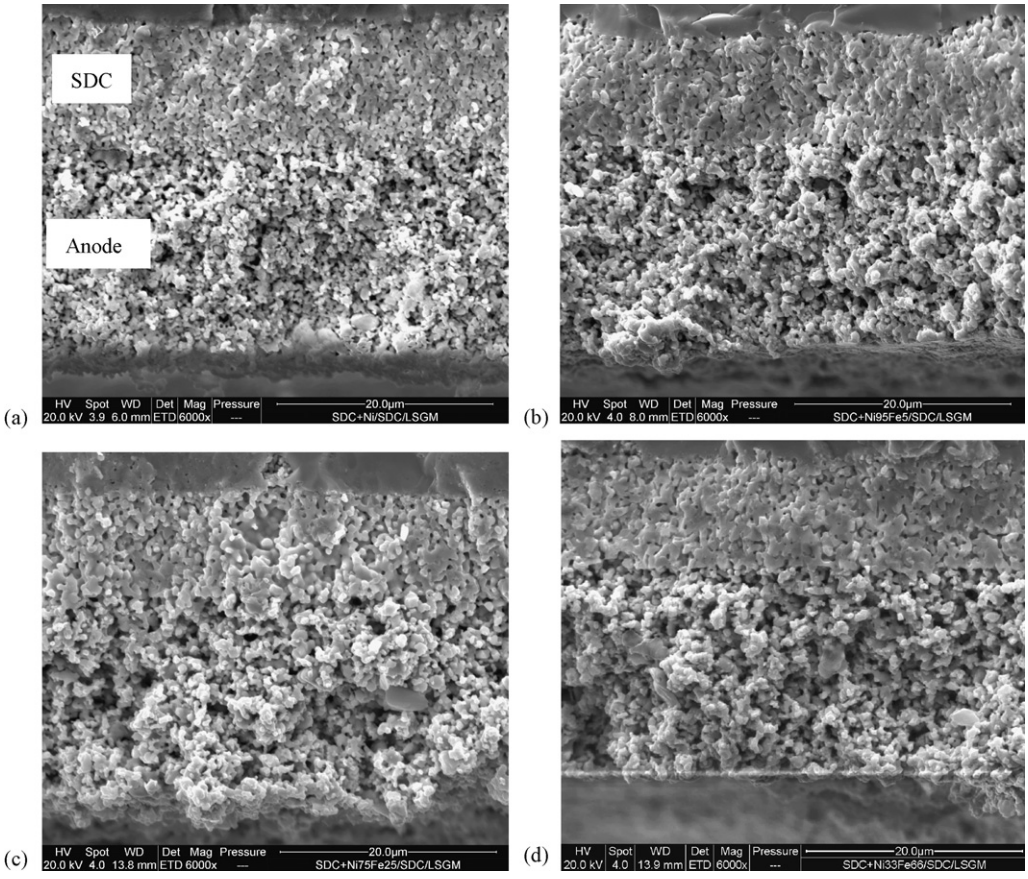

Fig. 2. SEM images of the cross sections of different Ni–Fe + SDC composite anodes: (a) Ni + SDC; (b) $Ni_{0.95}Fe_{0.05}$ + SDC; (c) $Ni_{0.75}Fe_{0.25}$ + SDC; (d) $Ni_{0.33}Fe_{0.67}$ + SDC.

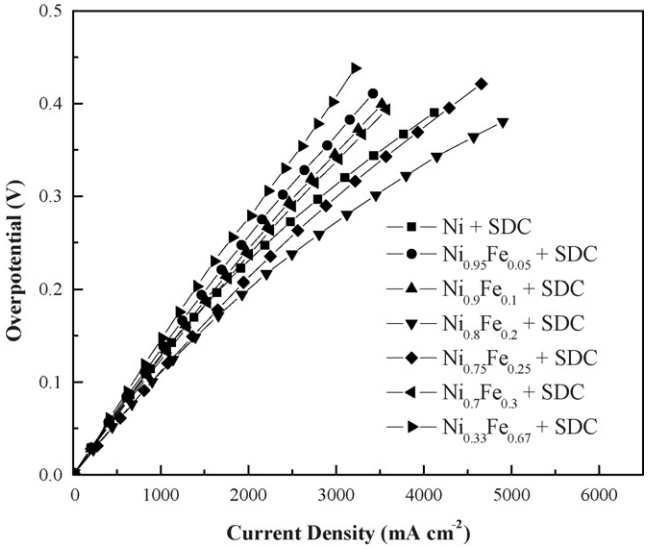

Fig. 3. Comparison in anodic overpotential of various Ni–Fe + SDC anodes at 800 °C in H_2 + 3% H_2O.

3.2. Comparison of the anodic properties of the Ni–Fe + SDC anodes

Fig. 3 compares the overpotentials of the Ni–Fe + SDC anodes at 800 °C with LSGM and SCF as the electrolyte and cathode, respectively. Both the $Ni_{0.80}Fe_{0.20}$ + SDC and $Ni_{0.75}Fe_{0.25}$ + SDC anodes exhibited lower overpotentials than the Ni + SDC anode. This implies that a proper alloying of Ni with Fe might give a higher activity towards H_2 oxidation. The anodic overpotentials of different Ni–Fe + SDC compositions are in the following order: $Ni_{0.8}Fe_{0.2}$ < $Ni_{0.75}Fe_{0.25}$ < Ni < $Ni_{0.7}Fe_{0.3}$ < $Ni_{0.9}Fe_{0.1}$ < $Ni_{0.95}Fe_{0.05}$ < $Ni_{0.33}Fe_{0.67}$. The overpotential results at the same current density of 2000 mA cm^{-2}, as shown in Fig. 4, indicate that the change of overpotential is opposite to that of power density with the increase in the addition of Fe. The power density of the cells reached a maximum as the metal composition got close to $Ni_{0.8}Fe_{0.2}$, while the anodic overpotential reached a minimum. Fig. 5 shows the

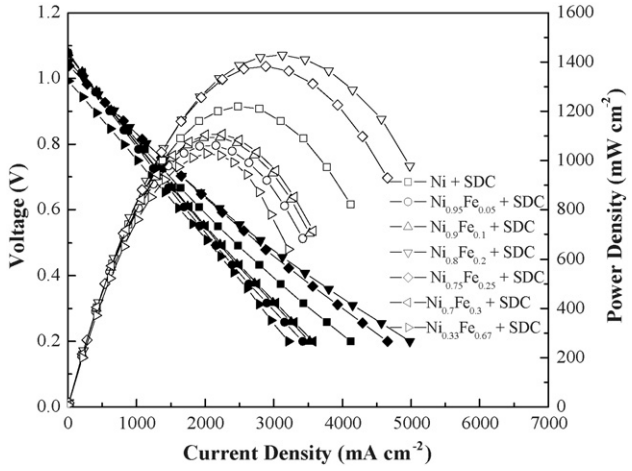

Fig. 5. Voltage and power density as a function of current density for single cells with different Ni–Fe + SDC anodes at 800 °C.

voltage and power density as a function of current density for single cells with different anodes, while Fig. 6 gives the cell performance with the $Ni_{0.8}Fe_{0.2}$ + SDC anode at different temperatures. The maximum power densities of the single cells with the $Ni_{0.8}Fe_{0.2}$ + SDC and $Ni_{0.75}Fe_{0.25}$ + SDC anodes at 800 °C in wet H_2 reached 1.43 and 1.38 W cm^{-2}, respectively. The cell with $Ni_{0.33}Fe_{0.67}$ + SDC exhibited the worst performance among all the studied anodes, which still reached about 1.03 W cm^{-2}. Since the electrolyte and cathode were prepared identically, the performance of these cells depended strongly on the anode composition.

The impedance spectra of single cells with various Ni–Fe + SDC anodes are shown in Fig. 7. All the data were obtained at 800 °C in wet H_2 under OCV. The high-frequency intercept of the impedance spectra corresponds to the ohmic resistance of the cell, including ohmic resistance of the LSGM electrolyte and the SDC buffer layer, ohmic resistance of the Ni–Fe + SDC anode and the SCF cathode, contact resistance at the electrode/electrolyte interface, and contact resistance between the electrodes and current collector [26]. The high-

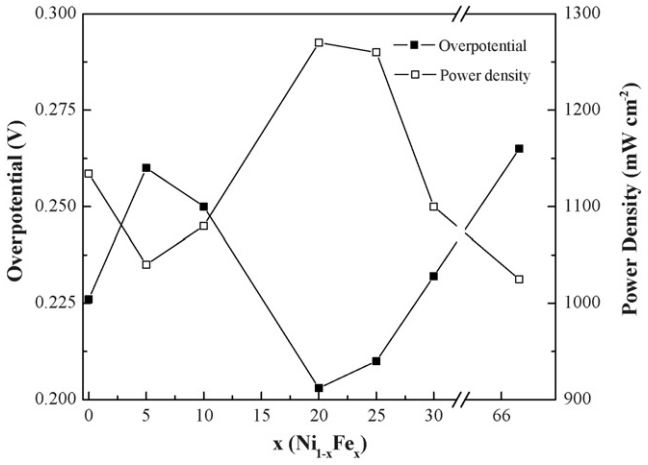

Fig. 4. Effect of alloy composition on the anodic overpotential and power density for single cells with a current density of 2000 mA cm^{-2} at 800 °C.

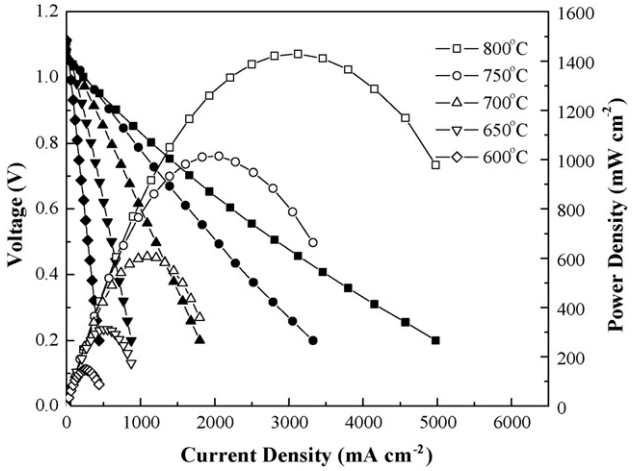

Fig. 6. Voltage and power density as a function of current density for a single cell with the $Ni_{80}Fe_{20}$ + SDC anode at different temperatures.

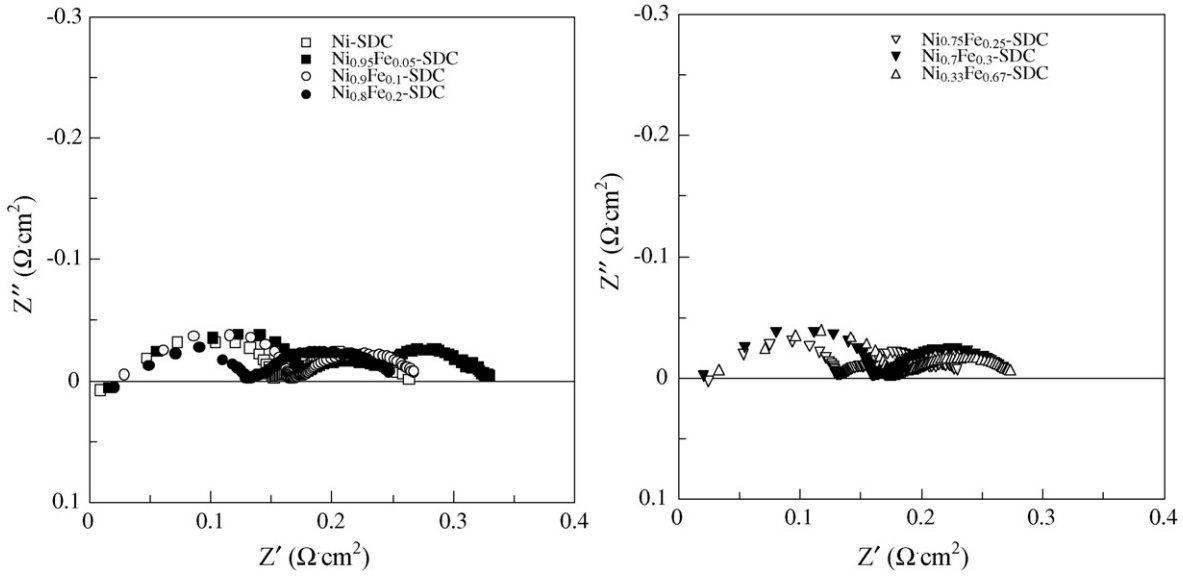

Fig. 7. Impedance spectra of single cells with different Ni–Fe + SDC anodes at 800 °C under OCV.

frequency and low-frequency depressed arcs are due to different electrode polarization processes. As mentioned earlier, the compositions and preparation conditions for the electrolyte and cathode, as well as the single cell fabrication steps, were identical for all the single cells; therefore, the cathodic polarization resistance and total ohmic resistance of the cells should be the same. Since the low-frequency arc remained essentially constant for the different cells, it was assigned to be from the cathode. On the other hand, the high-frequency arc changed significantly as the anode composition varied; therefore, it was related to the anodic process. The polarization resistances of different anodes were calculated from the high-frequency depressed semicircles, which increased from 0.105 Ω cm^2 for $Ni_{0.8}Fe_{0.2}$ + SDC to 0.265 Ω cm^2 for the $Ni_{0.33}Fe_{0.67}$ + SDC at 800 °C.

Fig. 8 presents the maximum power density and anodic overpotential as a function of anodic polarization resistance for the different cells at 800 °C. With the increase in anodic polarization resistance, the anodic overpotential increased and the maximum power density decreased accordingly. Clearly, anodic polarization resistance is the controlling factor in affecting the anodic overpotential and maximum power density for the Ni–Fe alloy anodes.

3.3. Long-term stability of the $Ni_{0.80}Fe_{0.20}$ + SDC anode

To evaluate an anode material, long-term stability is another important parameter.

To test the performance stability of the $Ni_{0.80}Fe_{0.20}$ + SDC anode, a single cell with this anode was run in wet H_2 with a fixed current density of 1875 mA cm^{-2} at 800 °C. As shown in Fig. 9, the power density dropped from 1271 to 1170 mW cm^{-2} after almost 160 h. The degradation in power was about 7.9%. Especially, from Fig. 9, it can be seen that the anodic overpotential increased slightly during the first 40 h and kept almost

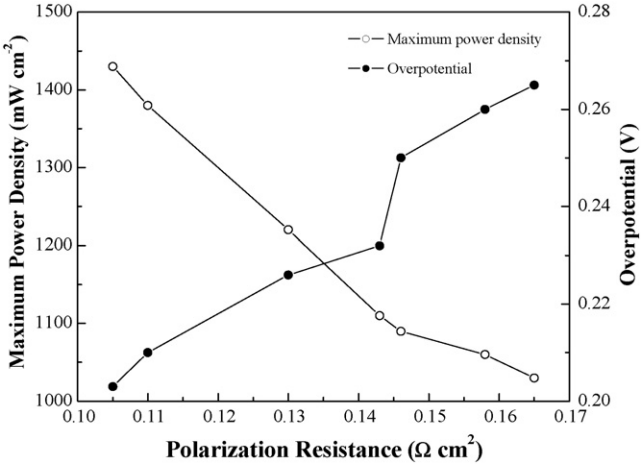

Fig. 8. Maximum power density and anodic overpotential as a function of anodic polarization resistance for single cells with different anodes.

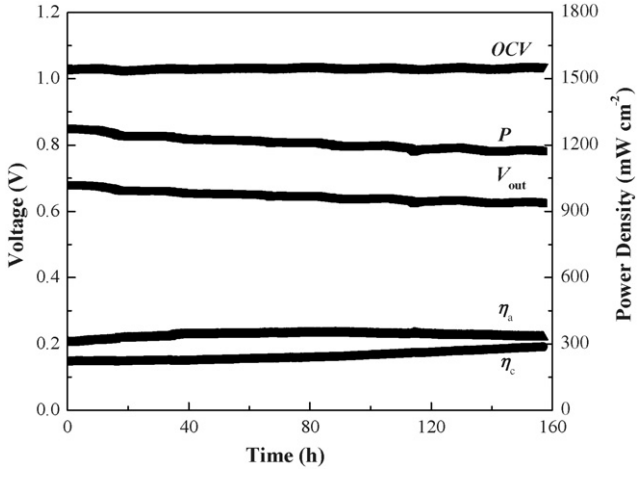

Fig. 9. Long-term stability of a ($Ni_{80}Fe_{20}$ + SDC)/SDC/LSGM/SCF single cell at 800 °C with a fixed current density of 1875 mA cm^{-2} (P, power density; V_{out}, output voltage; η_a, anodic overpotential; η_c, cathodic overpotential).

unchanged afterwards. The power drop after the initial 40 h was mainly due to the increase of cathodic overpotential. It seems that a buffer layer between the LSGM electrolyte and the SCF cathode is needed for improving the long-term cell stability.

3.4. Possible mechanism responsible for the "Fe" effect in the anode

With the addition of 5 wt.% Fe into Ni, the anodic overpotential increased from 0.226 to 0.260 V at the current density of 2000 mA cm^{-2} at 800 °C, as shown in Fig. 4. No Fe peaks were observed in the XRD patterns of the $Ni_{0.95}Fe_{0.05}$ + SDC composite anode after reduction at 800 °C, indicating that Fe atoms have dissolved into Ni to form an alloy, which may decrease the anode catalytic activity towards H_2 oxidation. According to Shinagawa et al. [22], a 5 wt.% of Fe added into Ni increased the activity of Ni in the anode reaction. Since impregnation was used for adding Fe to the Ni anode in their anode fabrication, the discrepancy might be due to the difference in anode fabrication process.

Based on the overpotential and power density data, the $Ni_{0.8}Fe_{0.2}$ + SDC anode exhibited the highest catalytic activity towards H_2 and the best performance among all the composite anodes. Wang and Gao [5] studied the Ni–Fe + LSGM composite anodes for DME fuel cells. Their results are in agreement with ours that an addition of 20–30 wt.% Fe into Ni improved its catalytic activity for fuel oxidation. The mechanism responsible for such superior performance for the $Ni_{0.8}Fe_{0.2}$ alloy anode is not clear at this stage. According to the Ni–Fe phase diagram [23], the Ni_3Fe phase will be present in these alloys at temperatures lower than 517 °C. The intermetallic phase, Ni_3Fe, possesses extraordinary catalytic ability towards H_2 decomposition in the ordered state [27]. However, at higher temperature (e.g. 600–800 °C as used in this study) it only exists as a disordered phase [23]. Indeed, if the $Ni_{0.8}Fe_{0.2}$ + SDC and $Ni_{0.75}Fe_{0.25}$ + SDC anode powders were reduced in H_2 + 3% H_2O at 800 °C and then immediately quenched to room temperature, a disordered Ni–Fe solid solution was detected, as shown in Fig. 1. Therefore, one postulation is that some short-range ordering might still exist in the disordered structure at higher temperature, which could lead to the enhanced catalytic performance for the $Ni_{0.8}Fe_{0.2}$ + SDC and $Ni_{0.75}Fe_{0.25}$ + SDC anodes.

Also, it was noticed that if $Ni_{0.8}Fe_{0.2}$ + SDC and $Ni_{0.75}Fe_{0.25}$ + SDC powders were reduced in Ar + 5% H_2 + 3% H_2O instead of H_2 + 3% H_2O, followed by immediate quenching to room temperature, a perovskite phase, $CeFeO_3$, was detected [28]. On the other hand, in the other compositions of Ni–Fe + SDC, no $CeFeO_3$ was observed. The $CeFeO_3$ phase is stable in a reducing atmosphere of O_2 partial pressures from about 10^{-22} to 10^{-15} atm at 800 °C and unstable in air by decomposing to CeO_2 and α-Fe_2O_3 [29–33]. Typically, the O_2 partial pressure at the anode side is about 10^{-22} atm. The partial pressure at the electrolyte/electrode interface may decrease a few orders of magnitude during the cell operation due to the O^{2-} transported from the electrolyte, which implies that $CeFeO_3$ may exist at the electrolyte/electrode interface. The presence of $CeFeO_3$ might also modify the catalytic properties of the composite anode. However, it is very difficult to identify the phases at the anode region near the electrolyte/anode interface *in situ* during cell operation. Clearly, more work is needed to further investigate the mechanism(s) responsible for the high performance of the $Ni_{0.8}Fe_{0.2}$ + SDC anode.

4. Conclusions

Ni–Fe + SDC composite anodes have been studied as anode materials for intermediate temperature SOFC. Among all of the composite anodes, the $Ni_{0.8}Fe_{0.2}$ + SDC anode exhibited the lowest polarization resistance (e.g. 0.105 Ω cm^2 at 800 °C under OCV). Single cell with the $Ni_{0.8}Fe_{0.2}$ + SDC anode exhibited the maximum power density of 1.43 W cm^{-2} at 800 °C and 0.62 W cm^{-2} at 700 °C, indicating improved electrochemical performance over Ni + SDC. The anodic polarization resistance was found to be the controlling factor in affecting the anodic overpotentials and the power densities of the cells. The low polarization resistance of the $Ni_{0.8}Fe_{0.2}$ + SDC and $Ni_{0.75}Fe_{0.25}$ + SDC anodes might be related to the unique bonding between Ni and Fe in this composition range. Another possible contribution might be the formation of the perovskite phase $CeFeO_3$ at the electrolyte/anode interface during cell operation.

Acknowledgement

This work was supported by a Faculty Research Grant, Tennessee Technological University. Additional funding was provided by the Advanced Portable Power Institute.

References

[1] K. Huang, R. Tichy, J.B. Goodenough, C. Milliken, J. Am. Ceram. Soc. 81 (1998) 2581.
[2] F. Zhao, A.V. Virkar, J. Power Sources 141 (2005) 79.
[3] Y. Lin, Z. Zhan, J. Liu, S.A. Barnett, Solid State Ionics 176 (2005) 1827.
[4] E.P. Murray, T. Tsai, S.A. Barnett, Nature 400 (1999) 649.
[5] S. Wang, J. Gao, Electrochem. Solid-State Lett. 9 (9) (2006) A395.
[6] H.S. Spacil, US Patent 3,558,360 (1970).
[7] A. Bieberle, L.J. Gauckler, Solid State Ionics 135 (2000) 337.
[8] B. De Boer, M. Gonzalez, H.J.M. Bouwmeester, H. Verweij, Solid State Ionics 127 (2000) 269.
[9] K. Huang, R. Tichy, J.B. Goodenough, J. Am. Ceram. Soc. 81 (1998) 2565.
[10] M. Feng, J.B. Goodenough, J. Solid State Inorg. Chem. 31 (1994) 663.
[11] T. Ishihara, H. Matsuda, Y. Takita, J. Am. Chem. Soc. 116 (1994) 3801.
[12] K. Huang, M. Feng, J.B. Goodenough, J. Am. Ceram. Soc. 79 (1996) 1100.
[13] K. Huang, R. Tichy, J.B. Goodenough, M. Schmerling, J. Electrochem. Soc. 143 (1996) 3630.
[14] Z. Bi, B. Yi, Z. Wang, Y. Dong, H. Wu, Y. She, M. Cheng, Electrochem. Solid-State Lett. 7 (2004) A105.
[15] K. Huang, M. Feng, J.B. Goodenough, J. Electrochem. Soc. 144 (1997) 3640.
[16] M. Feng, J.B. Goodenough, K. Huang, C. Milliken, J. Power Sources 63 (1996) 47.
[17] K. Eguchi, T. Setoguchi, T. Inou, H. Arai, Proceedings of the Solid Oxide Fuel Cell III, PV 93-4, The Electrochemical Society, Pennington, NJ, 1993, p. 494.
[18] S. Park, R. Cracium, J.M. Vohs, R. Gorte, J. Electrochem. Soc. 146 (1999) 3603.
[19] K. Huang, J. Wan, J.B. Goodenough, J. Electrochem. Soc. 148 (2001) A788.

[20] K. Huang, J. Wan, J.B. Goodenough, J. Mater. Sci. 36 (2001) 1093.
[21] A. Ringuedé, D.P. Fagg, J.R. Frade, J. Eur. Ceram. Soc. 24 (2004) 1355.
[22] M. Shinagawa, T. Ishihana, A. Kawakami, H. Nishiguchi, Y. Takita, Proceedings of the Solid Oxide Fuel Cell IX, PV 2005-7, The Electrochemical Society, Pennington, NJ, 2005, p. 1331.
[23] T.B. Massalski, H. Baker, J.L. Murray, L.H. Bennett, Binary Alloy Phase Diagram, ASM International, 1986.
[24] X. Wan, Y. Chen, A. Chen, S. Yan, Intermetallics 13 (2005) 454.
[25] J. Wan, J. Zhu, J.B. Goodenough, Solid State Ionics 177 (2006) 1211.
[26] Y. Leng, S. Chan, K. Khor, S. Jiang, Int. Hydrogen Energy 29 (2004) 1025.
[27] K. Sasaki, J. Tamura, M. Dokiya, Solid State Ionics 144 (2001) 233.
[28] J. Wan, X.C. Lu, J.H. Zhu, unpublished results, Tennessee Technological University, 2006.
[29] K. Kitayama, K. Nojiri, T. Sugihara, T. Katsura, J. Solid State Chem. 56 (1985) 1.
[30] L.B. Vedmid, V.F. Balakirev, E.B. Gorbunov, O.M. Fedorova, Y.V. Golikov, Russ. J. Phys. Chem. 73 (1999) 1883.
[31] M. Robbins, G.K. Wertheim, A. Menth, R.C. Sherwood, J. Phys. Chem. Solids 30 (1969) 1823.
[32] N. Kimizuka, T. Katsura, Bull. Chem. Soc. Jpn. 47 (1974) 1801.
[33] Y.D. Tretyakov, V.V. Sorokin, A.R. Kaul, A.P. Erastova, J. Solid State Chem. 18 (1976) 253.